Kobe University Repository : Kernel

PDF issue: 2025-12-05

Experimental Evaluation of Bistatic Ocean Wave Remote Sensing System by GPS

Cui, Jian

Kouguchi, Nobuyoshi

(Citation)
IEICE Transactions on Communications,97(2):519-527

(Issue Date)
2014

(Resource Type)
journal article

(Version)
Version of Record

(Rights)
copyright©2014 IEICE

(URL)
https://hdl.handle.net/20.500.14094/90002996

KOBE UNIVERSITY

PAPER

Experimental Evaluation of Bistatic Ocean Wave Remote Sensing System by GPS

Jian CUI[†], *Nonmember and* Nobuyoshi KOUGUCHI[†a)], *Member*

SUMMARY This paper presents an experimental evaluation of an ocean wave remote sensing system that uses bistatic GPS signal reflection to estimate wave characteristics. In our previous paper, a bistatic ocean wave remote sensing system by GPS was proposed to estimate the characteristics of sea swell near a harbor, and was also evaluated by numerical simulations. In the next phase, a prototype system has been developed and some basic experiments have been carried out in a coastal area in order to evaluate the system experimentally. In this paper, we will outline the prototype system. The system mainly consists of an array antenna, a front-end, and an estimator for ocean wave characteristics. Next, we explain that the estimator for ocean wave characteristics can identify each signal reflected from the ocean waves. Finally, the experiments show that the prototype system can receive the reflected signals from the sea-surface near the coast, and estimate the wave period and wavelength in the direction of the array antenna.

key words: *GSP signal, remote sensing, array antenna, front-end, ocean wave characteristics*

1. Introduction

Multipath is a phenomenon whereby a signal arrives at a receiver via multiple paths attributable to reflection and diffraction. In the general use of GPS, the multipath is a major source of error and degrades the accuracy of fixing a position. Performance improvements have been made by improving the characteristics of the antenna pattern, and the function of the receiver [1], [2]. Global Navigation Satellite System Reflectometry (GNSS-R) techniques have been developed to utilize the reflected GPS signals, as a kind of multipath from the sea-surface, to observe the sea state. Using the relative time delays and the power of the reflected signals, we are able to obtain a great deal of information about the sea-surface [3], [4]. Currently, the GNSS-R techniques are used to observe the sea state of a wide area, and techniques to measure detailed characteristics of ocean waves in a local area are not provided. Recently, some simulations and experiments have been carried out and indicated the possibility of measuring wave information of the local sea areas [5], [6].

In our previous paper, a method of bistatic ocean wave remote sensing system by GPS was proposed to estimate wave characteristics in a local area [7]. In this system, the Line of Sight (LOS) signal was received with a conventional antenna and passed to a front-end, then to a conventional receiver and a software receiver to obtain some satellite information such as azimuth and elevation angle of the satellite, a Doppler shift, and an arrival time of the LOS signal. On the other hand, the Reflected Signals From Sea-surface (RSFS) were received by an array antenna with a narrow beam-width, and sent to the Radio Frequency (RF) front-end which has a wide bandwidth (BW). After that, the correlators and the Teager-Kaiser Energy Operator (TKEO) [8] are combined to estimate the characteristics of the sea state. We were able to show that this system had the ability to estimate the wavelength and the wave period of the sea state, through numerical simulation. The next phase of this research called for a prototype system to be developed and some basic experiments carried out to evaluate the system performance.

In this paper, the prototype system is developed and applied in basic experimental evaluations. First, the array antenna [9], [10] was fitted with sixteen Left-Hand Circular Polarization (LHCP) patch antennas to obtain a narrow fan beam directional pattern so that signals reflected from the front side could be received while suppressing those from side directions. Next, a wide bandwidth front-end was built to separate and identify the reflected signals from each ocean wave on the sea surface. Finally, a wave characteristic estimator was developed to obtain the wave characteristics, such as ocean wave period and wavelength. A preliminary experiment was carried out to evaluate the prototype system, and the experimental results show that this ocean wave remote sensing system can identify the reflected signals from each ocean wave and estimate the wavelength and the period of sea surface near the coast.

2. Prototype System

2.1 System Configuration

Figures 1 and 2 respectively show the outline and the signal flow diagram of the prototype system. In Fig. 1, there are four GPS antennas. The upper GPS antenna and receiver are conventional and they receive the usual LOS signals from GPS satellites to obtain some satellite information such as the azimuth and the elevation angles of each satellite, Doppler shift and arrival time of each LOS signal. In the middle of the figure, there is an array antenna and two conventional GPS antennas. The two conventional antennas are used to measure the direction of the array antenna as a GPS compass. The array antenna is set in the direction of the objective satellite using the satellite information from

Manuscript received August 26, 2013.
Manuscript revised October 16, 2013.
[†]The authors are with the Graduate School of Maritime Sciences, Kobe University, Kobe-shi, 658-0022 Japan.
a) E-mail: kouguchi@maritimes.kobe-u.ac.jp
DOI: 10.1587/transcom.E97.B.519

Copyright © 2014 The Institute of Electronics, Information and Communication Engineers

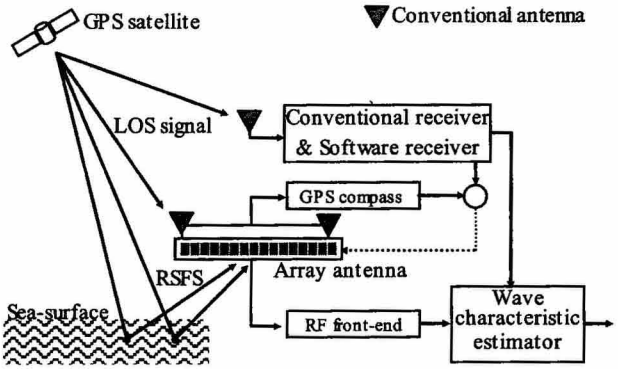

Fig. 1 Outline of prototype system.

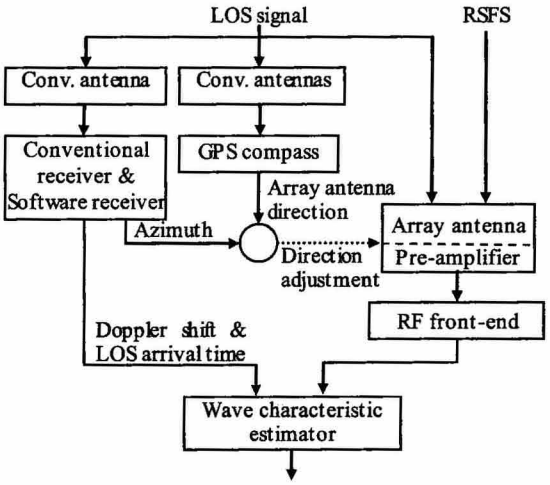

Fig. 2 Signal flow diagram of prototype system.

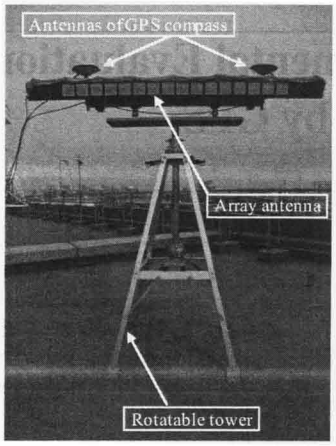

Fig. 3 Array and GPS compass antenna installed on rotatable tower.

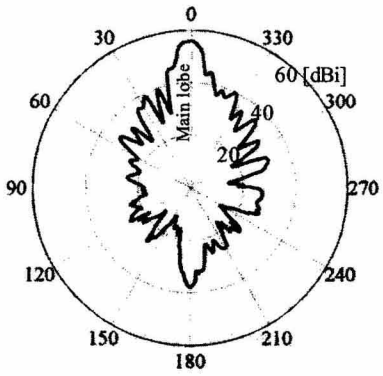

Fig. 4 Directional pattern of array antenna in horizontal plane.

the upper conventional GPS receiver and the directional information of the array antenna from the GPS compass, and simultaneously receives the LOS signal and the RSFS from the same satellite.

2.2 Array Antenna

An array antenna was developed to receive the RSFS of one visible satellite in a narrow beam-width. The signals are propagated from another direction to the array antenna have the same relative time delays as the desired RSFS, and the signals propagate from another direction interfere the desired RSFS. The array antenna can receive the RSFS in one direction and attenuate the interference from another direction.

In this array antenna, a uniform linear antenna array is made up of 16 elements of LHCP GPS patch antennas spaced in half wavelengths. The LHCP antenna was used since the polarization of the RSFS changes from right-hand circular polarization to LHCP [11], [12]. The bandwidth of the pre-amplifier in the array antenna is 40 MHz.

Figure 3 shows the array antenna installed on a rotatable tower with two conventional antennas which are used for the GPS compass. The directional pattern of the array antenna was measured in the electromagnetic wave anechoic chamber at the Furuno Electric Company. In the electromagnetic anechoic chamber, the one patch antenna transmitter emitted LHCP 110 dB (μV) 1575.5 MHz UHF signals. The array antenna was set 10 meters away from the transmitter. Figure 4 shows the directional patterns of the array antenna in horizontal plane by the dBi. From this figure, the narrow fan beam directional pattern can be seen.

The direction of the array antenna can be changed 360 degrees in the horizontal direction and 90 degrees in the vertical direction. The azimuth and the elevation angles of the objective satellite are obtained from the conventional GPS receiver, and the direction of the array antenna is derived from the GPS compass. Consequently, the direction of array antenna can be exactly adjusted to the objective satellite by comparing the two horizontal angles and the two vertical angles.

2.3 RF Front-end and Analog to Digital Conversion

The output signal of a RF front-end is limited by the bandwidths of the array antenna and the RF front-end. As the bandwidth of the array antenna is 40 MHz, 40 MHz can be selected as the bandwidth of the RF front-end at the maximum. In this section, the band-limited effect of the RF front-

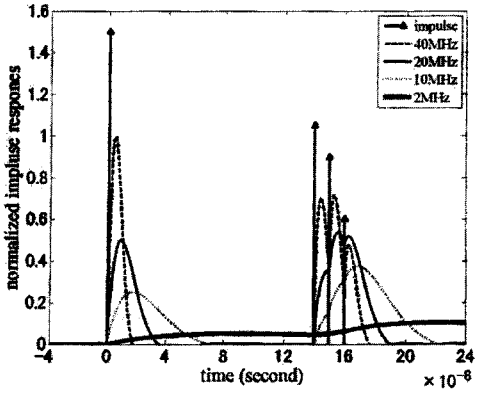

Fig. 5 Band-limited effects of RF front-end.

end and the role of the Analog to Digital (A/D) convertor are discussed.

The role of a RF front-end is to amplify the radio frequency signal and convert the radio frequency signal to an intermediate frequency (IF) signal. In a conventional GPS receiver, the bandwidth of the front-end amplifier is consistent with the transmitted signal bandwidth set to 2 MHz [13], [14]. However, a bandwidth of 2 MHz is not sufficient to identify each RSFS.

The band-limited effect of the front-end is shown in Fig. 5. In our previous paper, simulations were carried out to evaluate the proposed system performance [7]. In previous simulations, the LOS signal was initially received, and the first RSFS was delayed about 0.14 microseconds from the LOS signal. After the first RSFS, two RSFS were placed about 0.01 microseconds apart. At this front-end stage, with each delay time the LOS and the three RSFS form a four impulse function series. In this figure, the four band-limitted effects of the RF front-end are denoted using four different lines. From the results, the 2 MHz bandwidth wasn't sufficient to distinguish the LOS and RSFS, and even up to the bandwidth of 20 MHz we were unable to distinguish and identify each RSFS. At 40 MHz we could easily distinguish and identify each RSFS.

Consequently we chose 40 MHz as the bandwidth of the front-end. In this prototype system, the front-end (GP2015) made by Zarlink Semiconductor Inc. was used. In our front-end, the center frequency of the IF output signal is 175.42 MHz, and the bandwidth of the IF output is 40 MHz. The RF front-end output signal is sent to an A/D convertor.

The output signal of the front-end is sampled by the A/D convertor which has up to a 100 MHz sampling frequency. The 40 MHz bandwidth signal with 175.42 MHz center frequency is completely limited to the 4th Nyquist Zone. As a result, the under-sampling process translates the difference frequency component into the 1st Nyquist Zone from DC to 50 MHz (half of the sampling frequency) without aliasing [15]. Consequently, the center frequency of the A/D converter output is translated from the IF frequency 175.42 MHz to 24.58 MHz without aliasing by this A/D conversion.

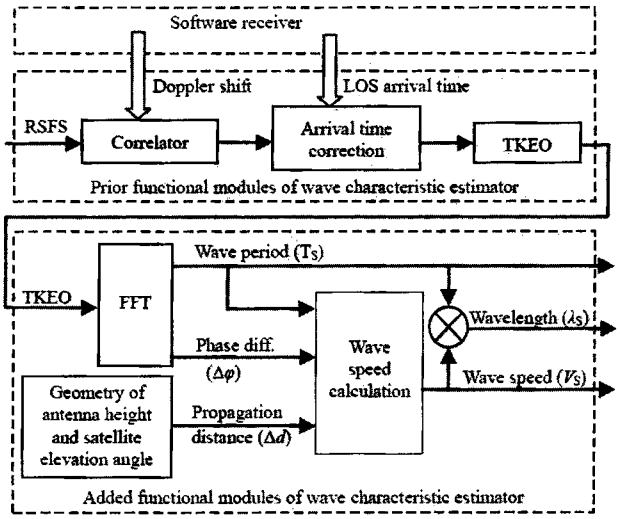

Fig. 6 Functional modules of wave characteristic estimator.

2.4 Wave Characteristic Estimator

The wave characteristic estimator is the most significant part of this prototype system, and estimates the wave period, the wave speed, and the wavelength of waves moving in the direction of the antenna array. The digital output signal is recorded by the hard disc drive. The recorded data is analyzed in the off-line mode.

Figure 6 shows the function modules of the wave characteristic estimator. The upper part of this figure shows the results from our previous paper where the wavelength and the wave period are already estimated in the TKEO output signals as prior functional modules [7]. In this prototype system, a quantitative method to estimate the wave characteristics is added in the lower part of the figure as added functional modules. The prior function modules are shown by the same expressions of our previous paper, and the added functional modules are newly proposed and explained to estimate the wave characteristics [7].

2.4.1 Prior Functional Modules

Each GPS satellite transmits a unique C/A code. Hence GPS receiver can detect GPS signals during satellite acquiring and code tracking. The correlation between two C/A codes is expressed as follows [7], [16],

$$r_i^{kk}(m) = \sum C^k(m_i)C^k(m)$$

$$and \quad \begin{cases} r_i^{kk}(m) \approx 0 & m \neq m_i \\ r_i^{kk}(m) = \frac{fs}{1000} & m = m_i \end{cases} \tag{1}$$

where r denotes correlation, k is the satellite number and i is the signal number, $C^k(m_i)$ and $C^k(m)$ are C/A codes, m_i and m are the numbers of samples for relative time delays to LOS signal, fs is sampling frequency. Usually $C^k(m)$ is

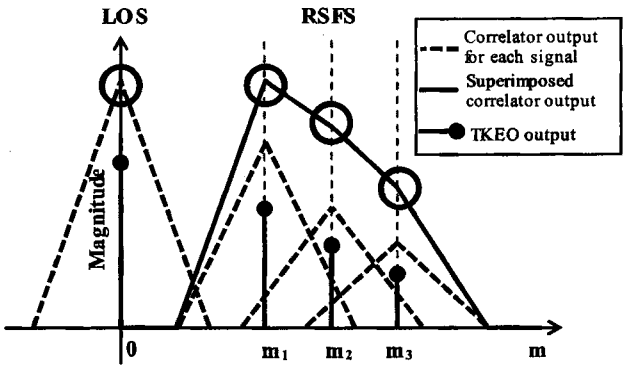

Fig. 7 Correlator and TKEO outputs.

locally generated code. A high correlation $fs/1000$ can be obtained because fs is much greater than 1000.

In Fig. 7, there are four GPS signals. One LOS signal is received at the zero position of the relative time delays (m = 0) with first one broken-line equilateral triangle peak, and three RSFS are received at the each relative time delays (m = m_1, m_2, m_3) with three broken-line equilateral triangle peaks. The total correlator output is obtained by superimposing these three correlator output signals of RSFS. Therefore the total correlator output of three RSFS is shown as the solid line. Each circle shows each peak point of the correlator outputs.

However, too much noise is included in the received signal so the peaks are hard to pick out from correlator output practically. Therefore, the discrete time TKEO that can be a high-pass filter [17] is used for identifying each peak of the correlator outputs. The TKEO for the correlator outputs shown in Fig. 7 is expressed as follows [7],

$$TKEO(m) = r^{kk}(m)^2 - r^{kk}(m-1)r^{kk}(m+1) \quad (2)$$

In Fig. 7, the TKEO outputs are denoted by four impulses at the respective relative time delay. In comparison between correlator outputs and TKEO outputs, the three outstanding peaks at m_1, m_2 and m_3 are obtained and each number of samples for relative time delay to LOS signal can be estimated clearly.

In Sect. 2.3, the band-limited effects of the RF front-end were explained; next the band-limited effects of TKEO outputs are examined with four GPS signals at each impulse position (shown in Fig. 5). In Fig. 8(a), there are four GPS signals. Figures 8(b)~(e) show the calculated TKEO outputs with 2, 10, 20, and 40 MHz bandwidths respectively. In Figs. 8(b)~(e), the white circles represent the TKEO outputs, and the black circles are the TKEO outputs at signal positions. In Fig. 8(b), the TKEO outputs steadily increase so that the remarkable values of TKEO outputs cannot be found. In Figs. 8(c) and (d), as each bandwidth of the RF front-end is not enough, we cannot adequately distinguish the black circles from others. In Fig. 8(e), the black circles can be clearly identified from the white circles using 40 MHz bandwidth. Consequently, the RF front-end 40 MHz bandwidth is the appropriate selection.

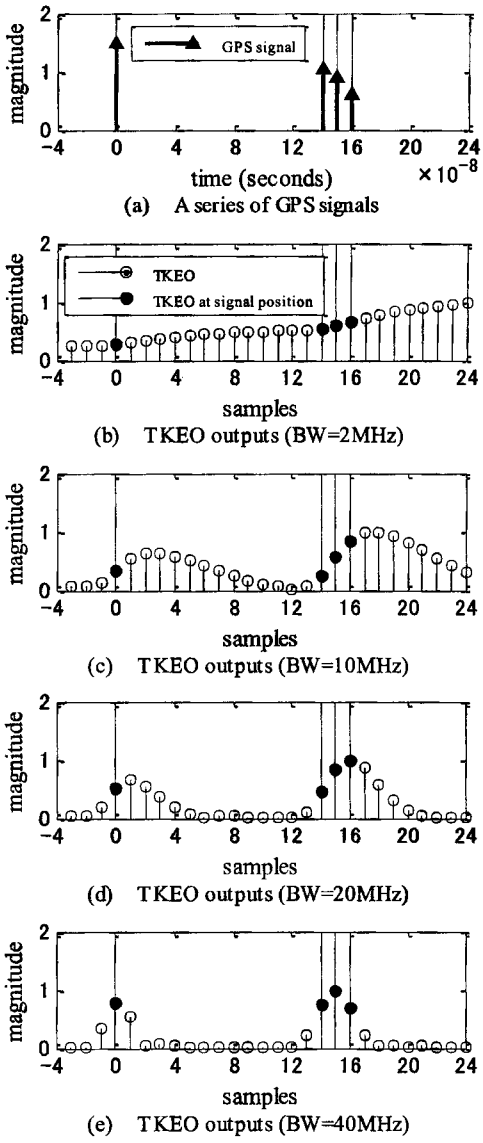

Fig. 8 Band-limited effects of TKEO outputs.

2.4.2 Added Functional Modules

In Fig. 6, the estimating functional modules of the wave characteristics are shown. In this section, each estimation module is expressed in detail. Firstly the calculation of the propagation that is necessary to obtain the wave speed is described, next each estimation method of three wave characteristics are explained in order.

(1) Propagation distance

For an estimation of the wave period and wavelength, each number of samples m_1, m_2 and m_3 are transferred to the distance from the array antenna to the reflection point. The horizontal distances from the array antenna to the reflection point are calculated using the geometry relationship of the antenna height and satellite elevation angle. Let h be the antenna height, E be the satellite elevation angle, c be light

speed, the horizontal distance, d, to antenna is calculated as follows [7],

$$d = h\tan\left(2\arctan\left(\frac{\frac{mc}{f_s h} - \sin E - \sqrt{\rho}}{1+\cos E}\right)\right)^{-1} \quad (3)$$

where, $\rho = (\frac{mc}{f_s h})^2 - \frac{2mc}{f_s h}\sin E$.

Next three horizontal distances to antenna (d_1, d_2, d_3) near the specular reflection sea area are selected to estimate the wave characteristics. The horizontal distance that is equivalent to the nearest sample number (m) around the specular reflection point is selected as d_1, and the horizontal distance that is equivalent to the next sample number in a direction away from the antenna site is selected as d_2 in order. Each horizontal distance resolution depends on the sampling frequency of the A/D converter.

(2) Wave period

In previous paper, it was shown that the strength of the TKEO outputs coincided with the strength of the reflected signals from the measureable sea-surface [7]. Accordingly, it is considered that the time series of each TKEO ($TKEO_t$) varies with the time change of the wave near specular reflection sea area. It is easy to find the wave period of the three $TKEO_t$ at three horizontal distances (d_1, d_2, d_3), but the Fast Fourier Transform (FFT) is needed to estimate the wave characteristics quantitatively. The wave period (T_S) near the reflected sea surface is estimated using the amplitude characteristics of the frequency transform. When the remarkable wave exists near specular reflection sea area, the wave period of the remarkable wave can be obtained using the amplitude characteristic by the FFT. When the wave does not exist, there is no significant peak in the amplitude characteristics.

(3) Wave speed

The wave speed is estimated using the phase characteristics of the frequency transform. Three phase values (φ_{d1}, φ_{d2} and φ_{d3}) at three horizontal distances (d_1, d_2, d_3) on the remarkable wave period are calculated by the FFT that is used to estimate the wave period. The phase difference ($\Delta\varphi_{d1,d2} = \varphi_{d2} - \varphi_{d1}$) between two adjacent phases of the $TKEO_t$ is equivalent to the propagation time ($\Delta t_S = T_S \times \Delta\varphi_{d1,d2}/2\pi$) that the ocean wave moves the distance ($\Delta d_{12} = d_2 - d_1$) from d_1 to d_2. Therefore the wave speed (V_S) can be estimated as following equation,

$$V_S = \frac{\Delta d_{ij}}{\Delta t_S} \quad (4)$$

From the dispersion relation of the ocean wave [18], [19], the wave speed can be calculated as

$$V_S = \frac{gT_S}{2\pi}\tanh(kz) \quad (5)$$

where g is the gravitational acceleration, k is the wave number, and z is the water depth.

(4) Wave length

The wavelength is calculated from the wave relationship between wave period (T_S) and wave speed (V_S) as follows,

$$\lambda_S = V_S \times T_S \quad (6)$$

From the dispersion relation, the wavelength can be calculated as

$$\lambda_S = \frac{gT_S^2}{2\pi}\tanh(kz) \quad (7)$$

3. Experimental Evaluation and Results

3.1 Experimental Conditions

The experiment was carried out on June 6th, 2012 with adequate wind and wave propagation from an approaching typhoon. Figure 9 shows the experiment site located on the Susami-coast of Wakayama Prefecture in Japan, and Fig. 10 shows the wave conditions of the reflection area on the sea. The array and GPS compass antenna unit was set on a hillside 110 meters above sea level, and marked by the white circle in Fig. 9. From this position, the measurable direction of the antenna is from 20 to 50 degrees. Three experiments, one in the morning, and two in the afternoon were carried out using different satellites and on differing ocean wave conditions. The conditions of the satellites and the ocean

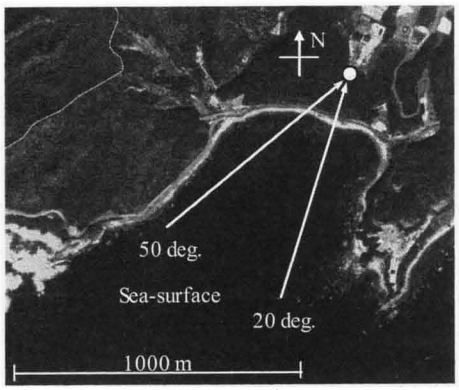

Fig. 9 Experiment site located on SUSAMI-coast. [Google Earth V7.0.3.8542. (March 28 2011). Susami Wakayama Japan. 33°33'3.22"N, 135°28'39.15"E, Eye alt 2.5 km.]

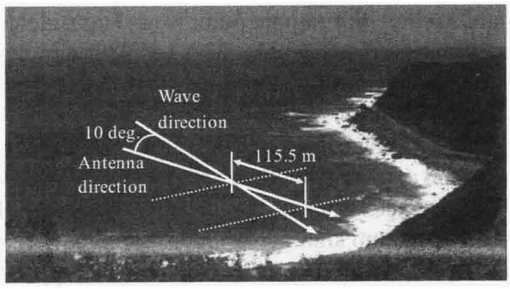

Fig. 10 Moderate wave condition near reflection sea-surface.

Table 1 Experimental conditions.

	experimental No.	1	2	3
time	recording time [s]	24	24	24
data	No. of samples [$\times 10^9$]	2.4	2.4	2.4
satellite	SV No.	21	22	22
	azimuth [deg.]	223	202	203
	elevation [deg.]	20	20	20
sea	state	smooth	moderate	moderate
	height [m]	-	1.5	1.5
	period [s]	-	11.5	11.5
	length [m]	-	115.5	115.5

waves are shown in Table 1. The first wave conditions were smooth, but in the second experiment the wave heights were 1.5 meters. The wave heights were estimated by sight, and the wave period of 11.5 seconds and the wavelength of 113.7 meters were measured from an image grab from the video footage of the experiment. The wavelength in the direction of the antenna was calculated by use of the difference angle between wave propagation and the direction of the antenna. In this experiment, as the difference angle was 10 degrees, the wavelength in the antenna direction was calculated to be 115.5 meters according to the cosine relation as $115.5 = 113.7 \div \cos(10)$. The elevation angle of the GPS satellites was 20 degrees. The direction of the array antenna was adjusted to the satellite direction using the GPS compass, and after that the output signals from the front-end were sampled and recorded.

3.2 Estimation of Wave Characteristics

In the first stage of the estimating process, the correlator, the arrival time correction and TKEO were performed as in the functional flow shown in Fig. 6. According to the quantitative method introduced in Sect. 2.4, the wave characteristics were estimated for smooth sea and moderate sea state respectively.

3.2.1 Smooth Sea State

In the first stage of the estimating process, the correlator and TKEO outputs of smooth sea state are shown in Fig. 11. The strong TKEO signal near the zero sample point of the vertical axis is the LOS signal, and the next strong TKEO signal near the 26th, 27th sample points are the RSFS. Figure 12 shows the top view of the aligned results of the averaged TKEO. In order to analyze the TKEO signals more fully, the signals at the 28th sample point is also considered. The horizontal distances at the 26th, 27th and 28th sample points are $d_1 = 348.0$, $d_2 = 444.0$ and $d_3 = 531.0$ meters from the array antenna position respectively.

Figure 13 shows three variations of each TKEO_t along the horizontal axis for smooth sea state. Figure 14 shows the amplitude characteristics of the TKEO_t by the FFT. In this figure, as there is no significant component, we cannot find the remarkable wave characteristics from these experimental results.

3.2.2 Moderate Sea State

Similarly, the correlator and TKEO output signals for moderate sea condition are shown in Fig. 15 and Fig. 16 shows the top view of the aligned results of the averaged TKEO. In these figure, three horizontal distances to the antenna (vertical axis: $d_1 = 348.0$, $d_2 = 444.0$ and $d_3 = 531.0$ meters) were selected to estimate the wave characteristics. Figure 17 shows three variations of each TKEO_t along the horizontal axis in moderate sea conditions, after that the variations of three TKEO_t are analyzed using the FFT. Figure 18 shows the amplitude characteristics of the TKEO_t, and the remarkable frequency of the wave is $f_0 = 0.083$ Hz (wave period is $T_S = 12.0$ seconds). Figure 19 shows the phase characteristics of the TKEO_t.

Figure 20 shows the phase change at three points of TKEO_t. In this figure, three phase values of the TKEO_t of the remarkable frequency ($f_0 = 0.083$ Hz) are drawn with three dots and the solid line is the regression line of the three points. From Eq. (4), the gradient of this line is the wave speed ($V_s = 10.6$ m/s). From Eq. (6), the wavelength (λ_S) is estimated to be 127.2 meters ($\lambda_S = 10.6 \times 12.0$). Meanwhile, the 12.0-second wave period and 114.1-meter wavelength were also calculated for the third experiment.

On the other hand from the Eqs. (5) and (7) of the dispersion relation, the wave speed and wavelength can be calculated using the wave period and the depth of water. The depth of the reflected sea area is about 10 meters. Hence in the experimental results, another estimation value of the wave speed and the wavelength can be calculated from the dispersion relation. From the wave period ($T_S = 12.0$ seconds) and the water depth ($z = 10.0$ meters), the wave speed (V_S) is 9.4 m/s and the wavelength (λ_S) becomes 113.2 meters.

Table 2 shows the experimental results for moderate sea state. In this table, the measurement values were obtained from the video grab, the estimation values were estimated by the prototype's system and the calculation values were obtained from the dispersion equation. The prototype system estimated the wave period, wavelength and speed in values virtually consistent with the measurement values and calculation values. The measurement values are not precise enough to analyze the estimation error, but the purpose of our research was to evaluate the usefulness of the prototype system and compare it with previous simulation results. From the experimental results, it is clear that our prototype system can be used to estimate ocean wave characteristics.

Next some factors affecting the estimation values are considered. The recording time of the experiments was too short to estimate the wave period precisely; as ocean waves have a lot of frequency components, the interference between the RSFS caused errors in the measurement phase; and as the signals from the specular reflection point to the array antenna had the same relative time delays as the RSFS, the signals having the same relative time delay, interfered with each other.

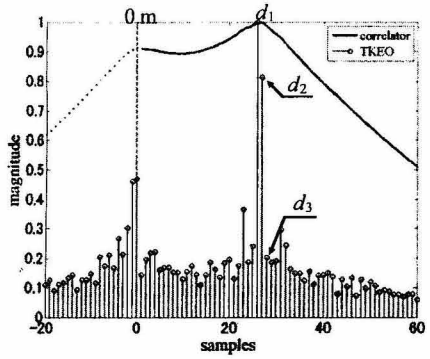

Fig. 11 Correlator and TKEO output signals (smooth).

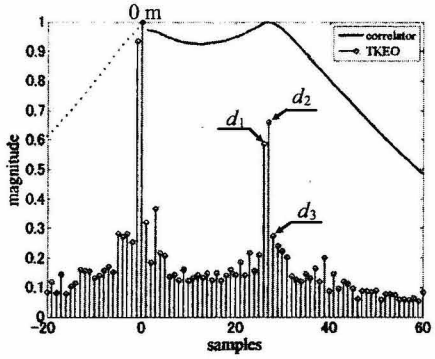

Fig. 15 Correlator and TKEO output signals (moderate).

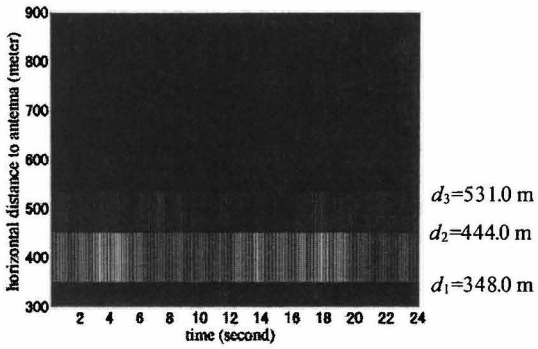

Fig. 12 Top view of aligned results of averaged TKEO (smooth).

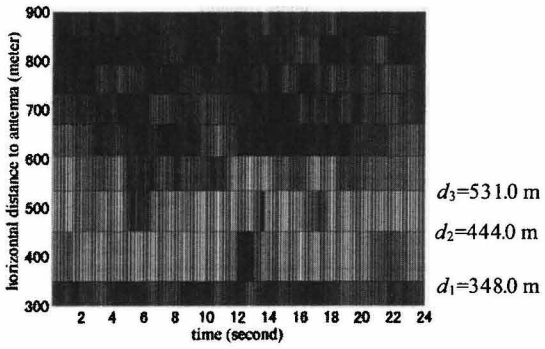

Fig. 16 Top view of aligned results of averaged TKEO (moderate).

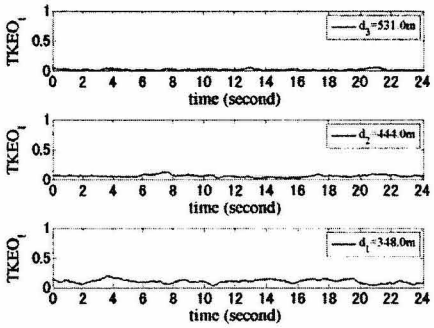

Fig. 13 Time variations of TKEO$_t$ (smooth).

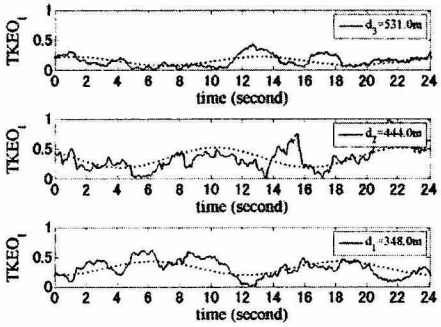

Fig. 17 Time variations of TKEO$_t$ (moderate).

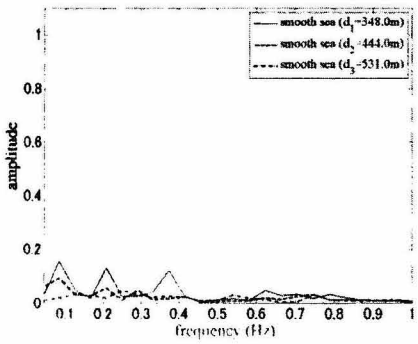

Fig. 14 Amplitude characteristics of TKEO$_t$ (smooth).

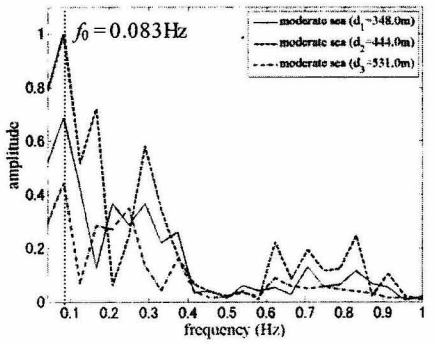

Fig. 18 Amplitude characteristics of TKEO$_t$ (moderate).

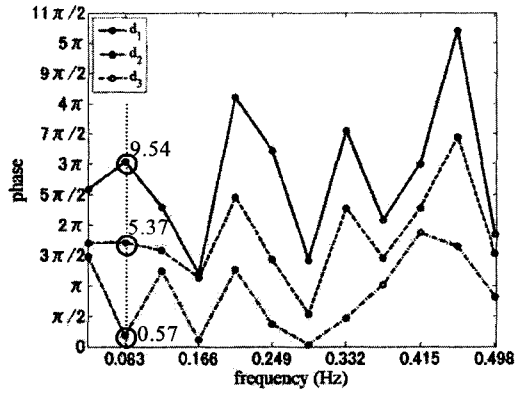

Fig. 19 Phase characteristics of $TKEO_t$ (moderate).

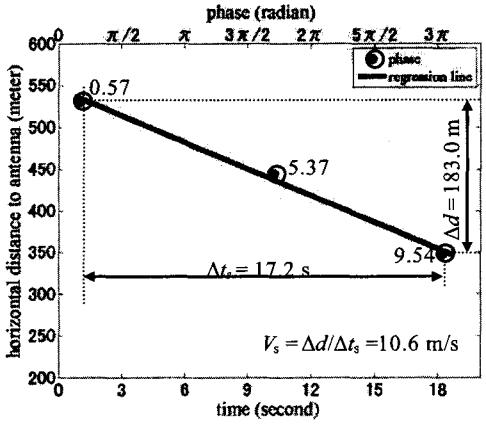

Fig. 20 Phase change at three points of $TKEO_t$ (moderate).

Table 2 Experimental results for moderate sea state.

Wave characteristics	Measurement from video grab	Estimation by prototype system		Calculation from dispersion relation
Experimental No.	-	2	3	-
Period [s]	11.5	12.0	12.0	-
Wavelength [m]	115.5	127.2	114.1	113.2
Speed [m/s]	10.0	10.6	9.5	9.4

3.2.3 Considerations and Proposals

In conclusion, some considerations and proposals for future research are described as follows,

(1) Distance resolution

By broadening the bandwidth of the array antenna pre-amplifier and the RF front-end amplifier, and raising the sampling frequency of the A/D converter, the resolution of distance scale can be increased.

(2) Time resolution

To increase the carrier to noise ratio, a more suitable amplifier should be used. By doing this, the averaging time will be reduced, and the resolution of time scale can be increased.

(3) Frequency resolution

In this prototype system, as the recording time was set to 24 seconds, the resolution of frequency scale was limited to 1/24 Hz. Accordingly by making the recording time 60 seconds, the resolution of frequency scale can be improved up to 1/60 Hz.

(4) Undesired signal

At the same distance from the border of the specular reflection point, the close and long distance areas have the same delay time from the LOS signal. The reflected signals from the close range area contaminate the reflected signals from the long rage area. By connecting an array antenna vertically we could reduce the vertical beam-width, and the undesired reflected signals could be suppressed.

(5) Wave height

In this experiment, we had only two experimental results of the moderate and smooth sea state, and the wave heights were estimated by sight. It is too small in number and inaccurate to evaluate the experimental results. In order to compare the estimated wave height with the actual wave height more precise measurements will be required.

(6) Comparative wave characteristics

In this paper, since the comparative wave characteristics were measured by means of a video grab taken near the coast, the accuracy of the comparative wave characteristics were less than perfect. In the near future, GPS buoys will be used to measure more accurately the wave characteristics, and the accuracy of the comparative wave characteristics will be dramatically improved.

4. Conclusion

In our previous paper, a bistatic GPS ocean wave remote sensing system was proposed and a simulation confirmed its good ability at estimating wavelength and wave period [7]. Consequently, in this paper, some important components of the prototype system have been constructed: the array antenna, the RF front-end, the A/D converter, and the wave characteristic estimator. The array antenna has been developed to obtain a narrow fan beam directional pattern to receive the reflected GPS signals from specified directions on the sea-surface while suppressing those from side directions. The RF front-end with a 40 MHz bandwidth and the A/D convertor with 100 MHz sampling frequency were used to identify the reflected signals from the sea surface.

In this paper our experimental results were used to evaluate the prototype system. The wave period and the wavelength near the objective sea-surface were estimated successfully. Additionally, the measurements can be performed under conditions of bad weather and low visibility. However in this prototype system, only waves that have a relative direction component to the array antenna can be estimated,

but the true wave characteristics could be estimated by setting up another system with an intersecting bore sight and this should be considered for future study.

Acknowledgments

The authors would like to acknowledge the help of Mr. Y. Kobayashi, President of the Furuno Labotech International CO., LTD, and Professor Y. Arai of Marine Technical College for the measurement of the directional pattern with the array antenna, and wish to thank Mr. A. Ikawa, Mr. K. Itani and all members of our research lab. for providing supports on experiments.

References

[1] B.R.K. Rao, A.D. Sarma, and Y.R. Kumar, "Technique to reduce multipath GPS signals," Current Science, vol.90, no.2, pp.207–211, 2006.
[2] T.R. Peres, "Multipath mitigation techniques suitable For low cost GNSS receivers," Instituto Superior Técnico, pp.20–56, Sept. 2008.
[3] A. Komjathy, M. Armatys, D. Masters, and P. Axelrad, "Developments in using GPS for oceanographic remote sensing: retrieval of ocean surface wind speed and wind direction," Proc. 2001 National Technical Meeting of The Institute of Navigation, pp.753–761, March 2001.
[4] A. Rius, J.M. Aparicio, and E. Cardellach, "Sea surface state measured using GPS reflected signals," Geophysical Research Letters, vol.29, no.23, pp.37-1–37-4, Dec. 2002.
[5] M.N. Manuel, C. Marco, J. Font-Rossello, S. Lannelongue, and C.S. Vallmitjana, "The PARIS concept: An experimental demonstration of sea surface altimetry using GPS reflected signals," IEEE Trans. Geosci. Remote Sens., vol.39, no.1, pp.142–145, Aug. 2002.
[6] Z. Xunxie, W. Xin, S. Lianjun, and S. Qiang, "First results of GNSS-R coastal experiment in China," Geoscience and Remote Sensing Symposium, pp.5088–5092, July 2007.
[7] J. Cui and N. Kouguchi, "Bistatic ocean wave remote sensing system by GPS," IEICE Trans. Commun., vol.E96-B, no.6, pp.1625–1632, June 2013.
[8] K. Eivind, "Signal processing using the Teager energy operator and other nonlinear operators," Candidatus Scient thesis, University of Oslo Department of Informatics, pp.15–30, 2003.
[9] Rajeswari Chatterjee, Antenna theory and practice, second ed., pp.86–97, New Age International, 1996.
[10] P.S. Naidu, Sensor array signal processing, pp.75–105, CRC Press, 2000.
[11] B.R. Rao, W. Kunysz, and R. Fante, GPS/GNSS antennas, Artech House, 2012.
[12] T. Hu, "Controlled indoor GPS signal simulation," University of Calgary, Department of Geometrics Engineering, 2006.
[13] Tsui, "Fundamentals of global positioning system receivers: A software approach," vol.173 of Wiley Series in Microwave and Optical Eng., John Wiley & Sons, 2005.
[14] NovAtel Inc., "Discussions on RF signal propagation and multipath," Calgary, Alberta, Canada, T2E 8S5, Feb. 2000.
[15] W.A. Kester, The data conversion handbook, pp.77–80, Newnes, 2005.
[16] K. Borre, D.M. Akos, N. Bertelsen, P. Rinder, and S.H. Jensen, "A software-defined GPS and galileo receiver: A single-frequency approach," pp.25–26, Springer, 2007.
[17] V. Kandia and Y. Stylianou, "Detection of sperm whale clicks based on the Teager-Kaiser energy operator," Applied Acoustics, vol.67, pp.1144–1163, 2006.
[18] R.S. Johnson, A Modern introduction to the mathematical theory of water waves, pp.62–64, Cambridge University Press, 1997.
[19] S.R. Massel, "Ocean surface waves: Their physics and prediction," World Scientific, pp.95–96, 1996.

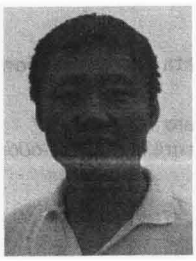

Jian Cui received the first Master's degree of Control Theory and Control Engineering in 2007 from Dalian Maritime University of China and the second Master's degree of Maritime Management Sciences in 2009 from Kobe University of Japan. Now, he is in pursuit of doctor's degree and his research field focuses on ocean wave observation by GPS signal.

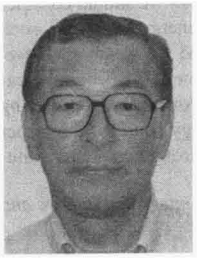

Nobuyoshi Kouguchi received B.Sc. Degree of Maritime Science in 1978 from Kobe University of Mercantile Marine, and Ph.D. degree of Communication engineering in 1998 from Osaka University. From 1979 to 1991, he worked as an assistant and associate professor at Maritime Technical College. From 1992 to 2000, he was an associate professor at Kobe University of Mercantile Marine. He is currently a professor of Graduate school of Maritime Sciences, Kobe University. His interesting researches are ocean measurement science and technology, global navigation satellite system, and decision-making process of mariner.